

Significance of high charge state of projectile ions inside the target and its role on electron capture leading to target ionization phenomenon

Soumya Chatterjee¹, Prashant Sharma², C.C. Montanari³, D. Mitra¹ and T. Nandi^{4*}

¹*Department of Physics, University of Kalyani, Kalyani, Nadia-741235, WB, India.*

²*Department of Particle and Astrophysics, Weizmann Institute of Science, Rehovot 76100, Israel*

³*Instituto de Astronomía y Física del Espacio, CONICET and Universidad de Buenos Aires, Buenos Aires, Argentina and*

⁴*Inter-University Accelerator Centre, Aruna Asaf Ali Marg, Near Vasant Kunj, New Delhi-110067, India.**

The K x-ray spectra of different targets (Cu, Zn, and Ge) induced by 3 to 5 MeV/u Si projectile ions have been measured to determine the K-shell ionization cross-section. A significant difference is observed between the measurements and theoretical estimates, with the latter being about 50% below the experimental results. This underestimation is attributed to the charge-exchange from target K-shell to projectile K- and L-shells. Such observation can only be possible if the projectile ions attain up to H- and He-like charge states. Corresponding projectile charge state fractions have been evaluated from the Lorentzian charge state distribution, where mean charge state is taken from the Fermi gas model [Phys. Rev. Lett. 30, 358 (1973)] and width from the Novikov and Teplova approach [Phys. Lett. A378, 1286–1289 (2014)]. The sum of the direct ionization cross-section and K-K + K-L capture cross-sections gives a good agreement with the measured cross-sections. Furthermore, we have validated this methodology with available data for Si-ion on Ti target. Such results may be useful in many solid target based applications.

I. INTRODUCTION

The study of ionization dynamics of target atoms by energetic heavy ions is critical in several fields of research such as material analysis, material engineering, atomic and nuclear physics, accelerator physics, biophysics, medical science, etc. The precise data of ionization cross-section of target atoms are required in case of heavy-ion application in particle-induced x-ray emission (PIXE) [1] and in heavy-ion tumor therapy [2]. Appropriate knowledge of K-shell ionization is essential to determine the elemental concentration during PIXE analysis and to estimate the direct damage of the tumor by the projectiles. Besides the target ionization, the effect of secondary electrons during heavy ion impact in the patient's body is very significant leading to much greater damage than the direct damage by the incident ions. The secondary electron yield is found to be proportional to the rate of energy loss of the incident particles [3], which again depends on the projectile charge state inside the target [4, 5]. Further, knowledge of the charge state of the projectile ions inside the target imparts a crucial role in electron capture processes leading to the inner shell ionization in the target atoms [6].

Though a monoenergetic beam with a fixed charge state is passed through the target material, a charge state distribution (CSD) of the projectile ions is manifested inside the target and being altered at the exit surface of the target before we measure it with the electromagnetic technique. This technique employs a dipole magnet, kept away from the target chamber, for dispersing the different charge states and a position sensitive detector at the

focal point to catch up all the dispersed ions. CSD of the coronal mass ejections has been measured by observatory borne charge analysers [7, 8] and theoretically studied [9]. Highly charged ions (HCIs) are prevalent in the inertial confinement fusion (ICF) [10]. The recent development of free electron laser has led to producing HCIs during x-ray-atom interactions and the CSD has been measured and theoretically interpreted [11–13]. The subject of this charge changing processes is thus significant.

Inner shell ionization by ion impact has been investigated in the laboratory with the availability of the accelerators since the 1950's [14]. A significant difference of ionization in gas and solid target was measured away from the target using a charge analyzer [15]. A vital role inside a target was put through a model associating the Auger processes which occur after the ions leave the solid [16]. Nevertheless, any direct measurement of the ionization phenomena inside the target was not possible until a couple of years ago [17]. Recently, it has been done using the x-ray spectroscopy technique [18]. The charge state of the projectile ion (q) in the beam-foil plasma created due to ion-solid interactions [19] is considerably higher than the measured ionic state outside the target [20] because of electron capture phenomena from the exit surface [21]. The problem of accurate charge states of ions inside solids is still a challenge in stopping power of ions in matter [22]. Such interesting features have not been exploited in the foil stripper technology to date.

Research on inner shell ionization of target atoms has been carried out for a long time with light as well as heavy projectiles (see for example [27–37]). This has enabled the research community to study processes like ionization, excitation, multiple ionization [23], radiative decay, Auger-decay [38], changes in atomic parameters, intrashell coupling effect [39, 40], etc at different energy regimes. Such processes occurring inside [18] as well as

* Email: nanditapan@gmail.com. Present address: 1003 Regal, Mapsko Royal Ville, Sector-82, Gurgaon-122004, India.

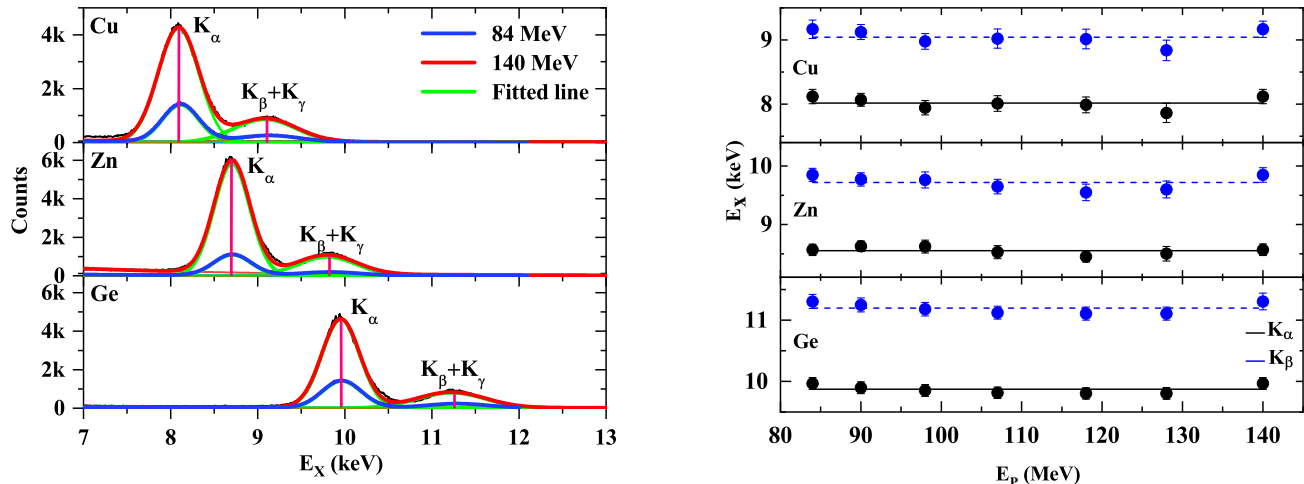


FIG. 1: Typical K x-ray spectra of natural Cu, Zn, and Ge targets when bombarded with 84 and 140 MeV ^{28}Si ions (left panel) and the x-ray peak energy shift in these targets as a function of the ion-beam energies of ^{28}Si ions (right panel). The solid and dotted orange lines in right panel show the mean value of the K_{α} and K_{β} peak energies.

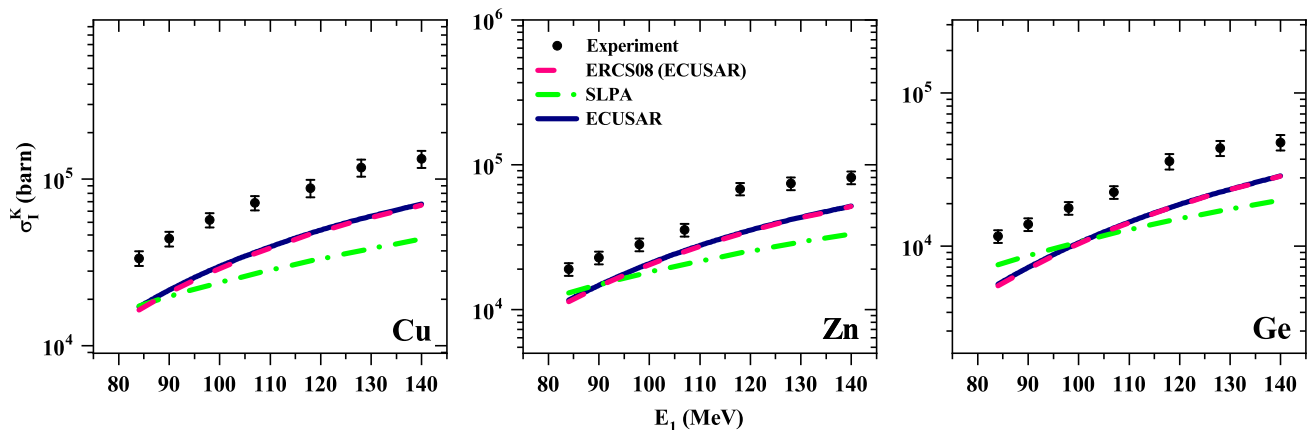


FIG. 2: Comparison of experimental K shell ionization cross-sections of different targets bombarded by the ^{28}Si ions as a function of ion-beam energies with the direct ionization cross-sections from ECUSAR [23], SLPA [24] and ERCS08 [25].

at the target surface [21] change the initial charge state of the projectile to several charge states. Thus, a CSD is measured by any set up placed away from the target. It is worth noting that the CSD depends on the initial parameters of the projectile ion (energy, initial charge state and atomic number) as well as target characteristics (thickness, density, and atomic number). Various groups have reported the CSDs using the techniques like the electromagnetic method [41], recoil separator [42, 43], TOF [44] and Coincident Rutherford Backscattering Spectrometry (CRBS) [45] to obtain the CSDs of the projectile outside the target, which has the combined effect of charge exchange processes in the bulk as well as the surface of the target. However, these techniques fail to separately

measure the CSD of the projectile inside and outside the solid target [5]. Theoretical studies include only the CSD outside the target as seen in several reviews [46–49], which include empirical models such as Bohr model [50], Betz model [16], Nikolaev-Dmitriev model [51], To-Drouin model [52], Shima-Ishihara-Mikumo model [53], Itoh model [54], and Schiwietz-Grande model [55]. However, theoretical models for estimating the CSDs inside the target are scarce, and this may be because of no concrete experimental guidelines up to now.

In the present work, we have measured the K-shell x-ray yields of target atoms in three projectile-target systems, i.e., Si + Cu, Si + Zn, and Si + Ge. Using K x-ray yields, we have determined the K-shell ionization

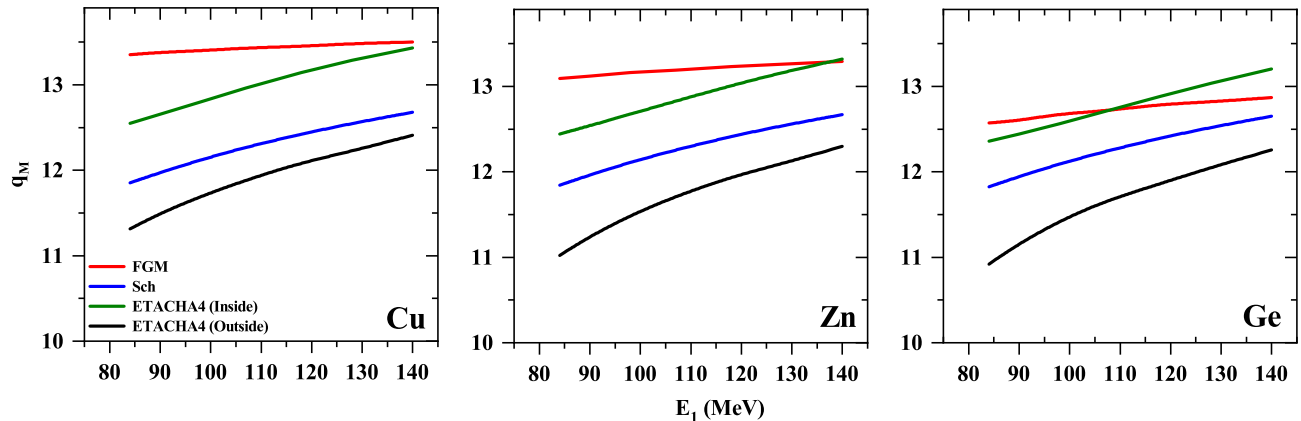


FIG. 3: Mean charge state of ^{28}Si ions inside the targets Cu, Zn, and Ge as predicted by the Fermi Gas Model (FGM) [56] and ETACHA4 (inside) are plotted against the incident energies. The same outside the targets as predicted by the Schiwietz-Grande model (Sch) [57] and ETACHA (outside) are shown as a function of the incident energies.

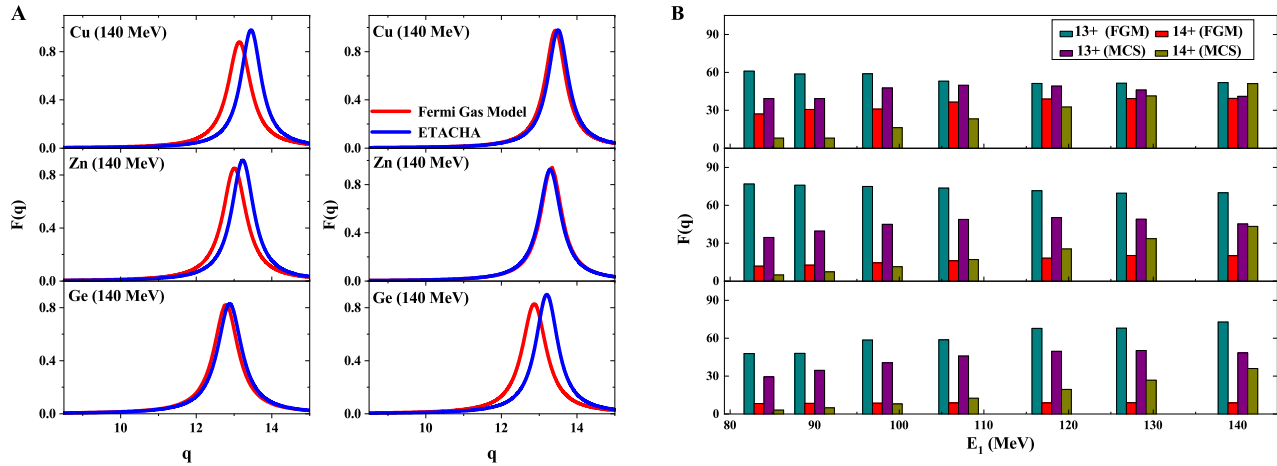


FIG. 4: A. Charge state distributions in side different targets according to the Fermi Gas Model (FGM) [56] and ETACHA4(inside) [58] at two select energies, B. Charge state fraction ($F(q)$) chart for $q = 13+$ and $14+$ inside the targets as a function of beam energies are also shown according to the Fermi Gas Model (FGM) [56] and ETACHA4(inside) [58].

cross-section of the target atoms. It is observed that the present measurements are about a factor of two higher than the theoretical direct ionization cross-sections. We have employed the Fermi-Gas model (FGM) [56] to determine the projectile charge-states inside the target material to explain the current findings in the light of electron capture induced target ionization [6]. We have found that the mean charge states predicted by FGM are close to theoretical estimates by the ETACHA4 code [58] provided the electron capture contribution is excluded. Using such mean charge states, the theoretical estimates of total ionization cross-section of targets are found to be in good agreement with the experimental measurements. Noteworthy here that the ETACHA4 code has never been

used or suggested to obtain the charge state distribution inside the solid target. We explored the fact that it has got required potentiality to do so. We have validated our theoretical method in a different system, Si ion on Ti target at 0.3 to 0.7 MeV/u energies [32]. Therefore, present work is appropriate enough for many applications as stated in the beginning.

II. EXPERIMENTAL DETAILS

The experiment was performed in the atomic physics beam line of 15 UD Pelletron which is situated at Inter-

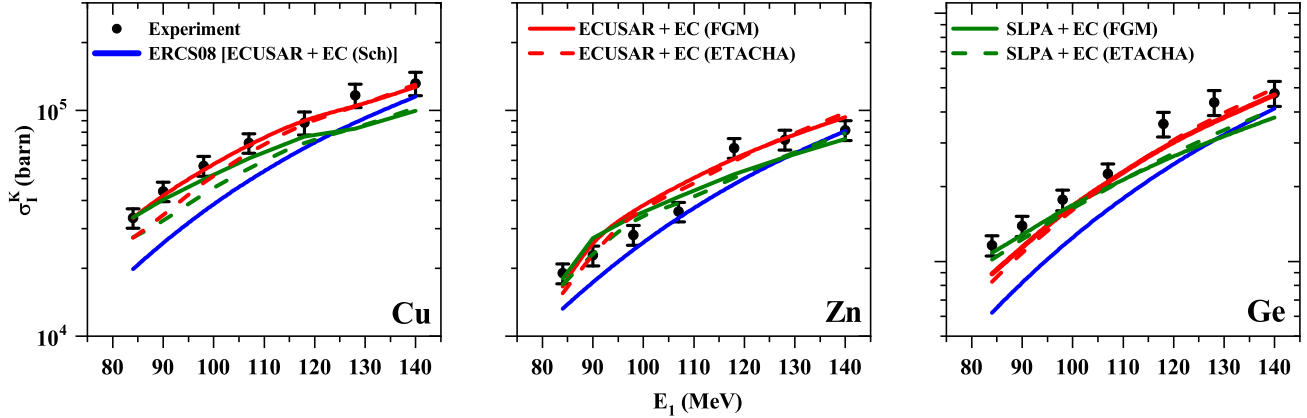


FIG. 5: Comparison of experimental K shell ionization cross-sections for different targets bombarded by the ^{28}Si ions as function of ion-beam energies with the sum of the direct ionization and K-K + K-L capture cross-sections. Here, the direct ionization cross-sections are taken from ECUSAR [23], SLPA [24], and ERCS08 [25]. While the electron capture cross-section is calculated from Ref. [59] and the charge state fractions of the projectile ions inside the target are taken from (i) ETACHA4 [58], (ii) Fermi gas model [56], which are denoted as EC(ETACHA4) and EC(FGM), respectively. Accordingly, we have represented different combinations of direct ionization and electron capture cross-sections in the figure.

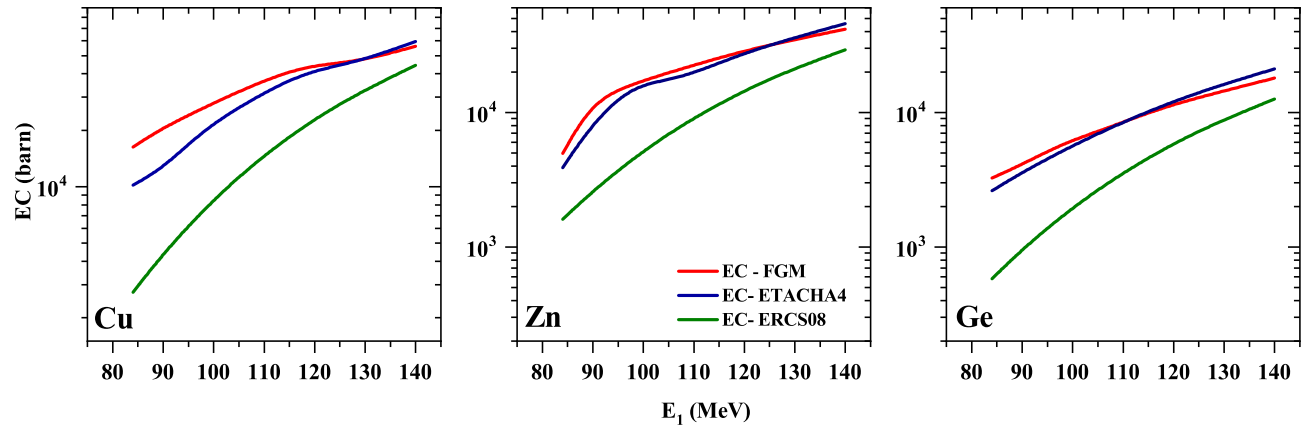


FIG. 6: Comparison of theoretical K-K capture cross-sections as calculated from Ref. [59] and the charge state fractions of the projectile ions are taken from (i) ETACHA4 [58], (ii) Fermi gas model [56] and (iii) ERCS08 [25]. We have represented such combinations as EC-ETACHA4, EC-FGM and EC-ERCS08, respectively.

University Accelerator Centre, New Delhi (India). Si ion beam of charge state 8^+ for beam energies 84, 90, 98, 107 MeV and charge state 12^+ for beam energies 118, 128, 140 MeV was obtained from Pelletron to bombard the natural Cu, Zn, and Ge targets. The vacuum of the order of 10^{-6} Torr was maintained in the chamber using turbo-molecular pump. Two silicon surface barrier detectors were placed at $\pm 7.5^\circ$ with respect to beam direction to normalize the charge. A Si(Li) solid state detector was placed outside the chamber at 125° with respect to beam direction and distance of 170 mm from the target. A collimator of 5 mm diameter was

placed in front of the detector inside the chamber. The thickness of the Mylar window of the chamber for the detector was $6\mu\text{m}$. The specification of the detector (ORTEC, Oak Ridge, Tennessee, USA) is as follows: thickness 5 mm, diameter 10 mm, the thickness of Be window $25\mu\text{m}$ and energy resolution 200 eV for Mn $K\alpha$ x-rays. The energy calibration of the detector was done before and after the experiment using the ^{55}Fe , ^{57}Co and ^{241}Am radioactive sources. The target surface was placed at 90° to the beam direction (normal to the target surface is collinear to the beam direction) on a rectangular steel ladder which could move horizontal and

TABLE I: Measured K shell production cross-sections (σ_k^x) for Cu, Zn, and Ge targets with corresponding multiple ionization probabilities, modified fluorescence yields for multiple ionization [23] and ionization cross-sections (σ_k^I) by ^{28}Si ions at different energies (E_1) (MeV). Single vacancy fluorescence yields (ω_k^0) for Cu, Zn, and Ge are 0.454, 0.486, and 0.546, respectively [26]. The cross-sections are in units of barns/atom.

Cu				
E_1	σ_k^x	P	ω_k	σ_k^I
84	27389±1415	0.817	0.819	33400±3340
90	34211±1767	0.766	0.780	43800±4380
98	41910±2160	0.705	0.738	56800±5680
107	50481±2580	0.649	0.703	71800±7180
118	69875±5329	0.590	0.670	88200±8820
128	89307±6786	0.547	0.647	117000±11700
140	97236±7343	0.501	0.625	132000±13200
Zn				
E_1	σ_k^x	P	ω_k	σ_k^I
84	15459±825	0.785	0.815	19000±1900
90	17851±947	0.736	0.782	22800±2280
98	21025±1107	0.680	0.747	28100±2810
107	25542±1337	0.626	0.717	35600±3560
118	46908±3675	0.571	0.688	68200±6820
128	49596±3865	0.529	0.668	74300±7430
140	53002±4115	0.486	0.648	81800±8180
Ge				
E_1	σ_k^x	P	ω_k	σ_k^I
84	9416±509	0.724	0.813	11600±1160
90	10959±589	0.679	0.789	13900±1390
98	13560±724	0.632	0.766	17700±1770
107	16684±877	0.581	0.742	22500±2250
118	30520±2397	0.534	0.721	35800±3580
128	36339±2846	0.495	0.704	43700±4370
140	38722±2994	0.456	0.688	47600±4760

vertical direction with the help of stepper motor. The spectroscopically pure (99.999%) thin targets of natural Cu, Zn, and Ge were made on the carbon backing using vacuum deposition technique. The thickness of Cu, Zn, Ge, and carbon backing was 25 $\mu\text{g}/\text{cm}^2$, 14.4 $\mu\text{g}/\text{cm}^2$, 99 $\mu\text{g}/\text{cm}^2$, and 20 $\mu\text{g}/\text{cm}^2$, respectively[?]. The thicknesses of targets were measured using the energy loss method using ^{241}Am radioactive source. The data was acquired using a PC based software developed at IUAC [61]. The beam current was kept below 1 nA to avoid pile-up effects and damage to the targets. A semi-empirical fitted relative efficiency curve used for the present measurement can be seen in Oswal et.al. [36].

III. DATA ANALYSIS, RESULT, AND DISCUSSION

Typical K x-ray spectra of Cu, Zn, and Ge bombarded with 84 MeV and 140 MeV Si ions are shown in Fig. 1. The spectra were analyzed with a nonlinear least-squares fitting method considering a Gaussian line shape for the x-ray peaks and a linear background fitting. The

TABLE II: Charge state fraction in % ($F(q)$) of Si^{13+} and Si^{14+} obtained from FGM [56], ETACHA4 [58] and ERCS08 [25] in different target elements and at various kinetic energies of Si-ion beam. Note that FGM and ETACHA4 represent $F(q)$ inside the target, while ERCS08 gives the same outside the target.

E_1	FGM		ETACHA		ERCS08	
	$F(13+)$	$F(14+)$	$F(13+)$	$F(14+)$	$F(13+)$	$F(14+)$
Cu						
84	61.0	27.0	39.2	7.9	19.5	2.4
90	58.6	30.7	39.2	7.9	22.9	3.1
98	58.8	30.9	47.6	16.3	27.5	4.3
107	53.0	36.4	49.7	23.1	32.5	5.8
118	51.2	38.9	49.1	32.6	37.9	7.8
128	51.3	39.2	46.1	41.3	42.2	9.9
140	51.8	39.4	41	51.1	46.4	12.6
Zn						
84	76.8	11.9	34.5	4.9	19.2	2.3
90	75.9	12.6	39.5	7.2	22.7	3.0
98	74.8	14.4	44.8	11.3	27.2	4.2
107	73.6	16.0	48.7	17.0	32.1	5.6
118	71.4	18.1	50.3	25.4	37.6	7.7
128	69.5	20.2	49.0	33.6	41.9	9.7
140	69.8	20.1	45.2	43.3	46.1	12.3
Ge						
84	47.8	8.3	29.4	3.2	18.7	2.2
90	47.9	8.4	34.5	4.8	22.1	2.9
98	58.5	8.6	40.6	7.9	26.6	4.0
107	58.6	8.7	45.9	12.4	31.5	5.4
118	67.7	8.7	49.6	19.5	36.9	7.4
128	67.9	8.9	50.2	26.8	41.2	9.3
140	72.8	8.8	48.3	36.0	45.6	11.9

x-ray production cross-sections for the K x-ray lines were determined from the relation,

$$\sigma_i^x = \frac{Y_i^x A}{N_A \epsilon n_p t \beta} \quad (1)$$

here Y_i^x is the intensity of the i th x-ray peak ($i = K_\alpha, K_\beta$). A is the atomic weight of the target. N_A and n_p denote the Avogadro number and the number of incident projectiles, respectively. ϵ , t , and β represent the effective efficiency of the x-ray detector, the target thickness in $\mu\text{g}/\text{cm}^2$, and the correction factor for energy-loss of the incident projectile and absorption of emitted x-rays in the target element, respectively. The sum of $\sigma_{K_\alpha}^x$ and $\sigma_{K_\beta}^x$ gives a measure of the total K x-ray production cross-section as given in Table I.

It is now well known that heavy ions produce simultaneous multiple ionization (SMI) in several shells while traveling through the target. SMI of L-shells along with a vacancy in K-shell will influence the value of K-shell fluorescence yield (ω_k) to a considerable extent. Instead of using rigorous Hartree-Fock-Slater calculation for the K_α and K_β peak shift due to the SMI effect, we employ a simple model of Burch et al. [62]. According to

TABLE III: Theoretical direct ionization cross-sections obtained from ECUSAR (DI_1), SLPA (DI_2), and ERCS08 (DI_3) are given. Theoretical K-K capture cross-sections have been calculated using Ref. [59] and for the Si projectiles of charge state 13+ and 14+. Total capture cross-section taking charge state fraction (F(q)) of 13+ and 14+ from FGM [56] (EC_1), ETACHA4 [58] (EC_2) and ERCS08 [25] (EC_3) are also listed. Finally, sum of direct ionization cross-section and total capture cross-section and experimental ionization cross-sections (σ_K^I) for *Cu*, *Zn* and *Ge* targets with about 10% uncertainty by the ^{28}Si ions of different energies (E_1 MeV) have been provided too. All the cross-sections are given in units of barns/atom.

E_1 (MeV)	DI_1	DI_2	DI_3	EC_1		EC_2		EC_3	$DI_1 +$ EC_1	$DI_1 +$ EC_2	$DI_2 +$ EC_1	$DI_2 +$ EC_2	$DI_3 +$ EC_3	σ_K^I (Exptl.)
				K-K	K-L	K-K	K-L							
Cu														
84	17080	17280	16400	12241	4037	5974	4197	2728	33358	27251	33558	27451	19808	33400
90	21630	19710	20860	15621	4997	7357	5179	4377	42248	34166	40328	32246	26007	43800
98	28400	23110	27460	19945	6465	13438	6672	7575	54810	48510	49520	43220	35975	56800
107	36503	27140	35660	25896	8283	20046	8593	12700	70682	65141	61319	55778	49203	71800
118	47540	32340	46500	33385	10954	29700	11315	21250	91879	88555	76689	73355	68790	88200
128	58041	37320	56820	32132	13692	31687	14072	30930	103865	103800	83144	83079	88971	117000
140	70864	43550	59460	38751	17393	41658	17748	44300	127008	130270	99694	102956	115164	132000
Zn														
84	11617	13030	11330	2042	2927	857	3030	1612	16586	15504	17999	16917	13229	19000
90	14825	14900	14500	8654	3612	4607	3751	2612	27091	23183	27166	23258	17437	22800
98	19680	17530	19310	11750	4696	11460	4851	4591	36126	35991	33976	33841	24271	28100
107	25819	20640	25400	14665	6093	11321	6275	7842	46577	43415	41398	38236	33661	35600
118	34077	24670	33630	19409	8041	17709	8298	13420	61527	60084	52120	50677	47497	68200
128	42082	28540	41610	23602	10076	24088	10377	19920	75760	76547	62218	63005	62002	74300
140	52035	33390	51560	28761	12803	32721	13145	29180	93599	97901	74954	79256	81215	81800
Ge														
84	5636	7550	5499	1834	1433	1027	1603	583	8903	8266	10817	10180	6219	11600
90	7301	8697	7140	2313	1787	1588	1933	957.2	11401	10882	12797	12278	8258	13900
98	9889	10270	9707	3529	2368	2607	2599	1721	15786	15095	16167	15476	11610	17700
107	13269	12170	13060	4588	3097	4194	3388	3028	20954	20851	19855	19752	16297	22500
118	17980	14630	17760	6796	4207	6810	4523	5380	28983	29313	25633	25963	23360	35800
128	22709	17010	22480	8525	5328	9779	5699	8267	36562	38187	30863	32488	30976	43700
140	28791	20000	28560	11120	6896	13791	7305	12610	46807	49887	38016	41096	41401	47600

it, the energy shift of K_α and K_β lines per $2p$ vacancy with respect to corresponding diagram lines are $1.66Z_L$ and $4.18Z_L$ eV, respectively, where $Z_L = Z_2 - 4.15$; Z_2 is the atomic number of the target element. It is clear from Fig. 1 (a) that K_α and K_β lines are well resolved for all the targets used in present measurements. In order to visualize the centroid shift due to the SMI effect, we have plotted the K_α and K_β energies versus beam energy for all the targets in Fig. 1(b). We notice, for all the targets, the corresponding centroid energies do not vary much with the beam energies used. The average K_α peak energies of *Cu*, *Zn*, and *Ge* are 8.01 ± 0.1 , 8.55 ± 0.1 , and 9.87 ± 0.1 keV, respectively and are close to the corresponding diagram K_α lines at 8.03, 8.62, 9.86 keV. In contrast, this picture for K_β lines is rather distinctive. Mean of the measured K_β lines 9.04 ± 0.13 , 9.72 ± 0.12 , and 11.2 ± 0.1 keV for *Cu*, *Zn* and *Ge*, respectively are higher than the corresponding diagram K_β lines at 8.905, 9.572, and 10.982 keV. Thus, the difference between the measured K_β and the diagram K_β lines for *Cu*, *Zn*, and *Ge* are 135, 148, and 218 eV, respectively. These values are somewhat larger than the energy shift per $2p$ vacancy for K_β lines, which are 104, 108, 116 eV, respectively, for *Cu*, *Zn*, and *Ge*. This figure along with the measurement

uncertainty mentioned above implies that on the average two vacancies occur in $2p$ shells during the present collisions. This picture corroborates well the scenario in the K_α case too as the energy shift per $2p$ vacancy in *Cu*, *Zn* and *Ge* for K_α line are only 41, 43, 46 eV, respectively, and the energy shift due to two $2p$ vacancies will be smeared in its measurement uncertainty of about 100 eV. Thus the SMI must be included in data analysis.

Theoretically, K x-ray production cross-section (σ_K^x) can be obtained using the relation [29]

$$\sigma_K^x = \omega_K \sigma_K^I \quad (2)$$

here σ_K^I is K-shell ionization cross-section, ω_k is the K shell fluorescence yield in the presence of SMI effect in L-shell. Single vacancy fluorescence yield ω_k^0 given by Krause [26] has been used. Hence, to extract the K shell ionization cross-section from the measured x-ray production cross-section one needs the accurate knowledge of ω_K . To estimate it amidst the SMI process discussed above, we are following the description of Lapicki *et al.* [23] using an assumption that each electron in a manifold of outer subshells is ionized with an identical probability

P and correct ω_K in presence of SMI process becomes

$$\omega_k = \frac{\omega_k^0}{1 - P(1 - \omega_k^0)}. \quad (3)$$

With

$$P = q_m^2 \left(1 - \frac{0.225}{v_1^2}\right) \times \frac{1}{1.8v_1^2} \quad (4)$$

here $v_1 = 6.351[E_1/A_1]^{1/2}$ (E_1 and A_1 are projectile energy and mass in MeV and amu units, respectively) is the projectile velocity. q_m is the mean charge state of the projectile ion inside the target.

The uncertainty in ω_k can be estimated from the following expression

$$\frac{\Delta\omega_k}{\omega_k} = \frac{\Delta\omega_k^0}{\omega_k^0} + \frac{P}{[1 - P(1 - \omega_k^0)]} \times \left[\frac{\Delta P}{P} \times (1 - \omega_k^0) - \frac{\Delta\omega_k^0}{\omega_k^0} \right] \quad (5)$$

where

$$\frac{\Delta P}{P} = \frac{2\Delta q_1}{q_1}. \quad (6)$$

The projectile velocity v_1 can be defined very precisely and thus its uncertainty is nominal ($< 1\%$) and taken as just a constant here. For Cu, $\frac{\Delta\omega_k^0}{\omega_k^0}$ is $\approx 5\%$ assume and this is $\approx 3\%$ for Zn and Ge. If we assume $\frac{\Delta q_1}{q_1}$ is $\approx 3\%$ (its estimation and probable uncertainty will be discussed later), $\frac{\Delta\omega_k}{\omega_k}$ turns out to be $\approx 6\%$.

The inner-shell vacancies are produced predominantly by the direct Coulomb ionization process, which can be treated perturbatively using the first-order perturbation approaches, namely, the plane-wave Born approximation. PWBA [63]. The standard PWBA approach for direct ionization were further developed to include the hyperbolic trajectory of the projectile, the relativistic wave functions, and the corrections for the binding-polarization effect. The most advanced approach based on the PWBA, which goes beyond the first-order treatment to include the corrections for the binding-polarization effects within the perturbed stationary states (PSS) approximation, the projectile energy loss (E), and Coulomb deflection (C) effects as well as the relativistic (R) description of inner-shell electrons, is known as the ECPSSR theory [64]. This theory is further modified to replace the PSS effect by a united and separated atom (USA) treatment and valid in the complementary collision regimes of slow and intermediate to fast collisions, respectively [23].

The shell wise local plasma approximation (SLPA) [24, 65] is an ab-initio approach for the calculation of ionization probabilities within the dielectric formalism. It is based on the quantum dielectric response theory, generally employed to deal with the conduction band of solids,

extended to account for the inner-shells by considering the density of target electrons and the binding energies. The SLPA calculates the K-shell ionization cross-section of certain target atom due to the interaction with a projectile (velocity v_1 and nuclear charge Z_1) as

$$\sigma_K^{SLPA} = 2/(\pi v_1^2) \int_0^\infty \frac{Z_1^2}{p} dp \int_0^{pv_1} d\omega \int Im\left[\frac{-1}{\epsilon(p, \omega, E_K, \delta_K(r))}\right] d\vec{r}, \quad (7)$$

with $\epsilon(p, \omega, E_K, \delta_K)$ being the Levine-Louie dielectric function [66], E_K the binding energy, $\delta_K(r)$ the density of the K-shell electrons around the nucleus, and p (ω) the momentum (energy) transferred. For Cu, Zn and Ge, we obtained E_K and $\delta_K(r)$ from the Roothaan-Hartree-Fock wave functions of neutral atoms by Clementi and Roetti [67]. These are the only inputs for our calculations. The SLPA has been successfully employed to describe the different moments of the energy loss of ions in matter, like ionization cross-sections of the L-shell [34, 36], K-shell ionization [29, 68], or mean energy loss [69, 70].

About a decade ago, Horvat [25] developed a FORTRAN code (ERCS08) for computing the atomic electron removal cross-sections (ERCS). The calculations are based on the ECPSSR theory for direct ionization and subsequent modifications, while the non-radiative electron capture is accounted by following Lapicki and McDaniel [6], Lapicki and Losonsky [59]. The ERCS08 program allows for selective inclusion or exclusion of individual contributions to the cross-sections. Thus, one can evaluate the K-shell ionization cross-section originated from direct ionization and nonradiative electron capture separately.

In Fig. 2, the measured σ_K^I are compared with the predictions of direct ionization cross-section from ECUSAR, SLPA, and ERCS08, calculated as mentioned above. As it can be noted, the ECUSAR and ERCS08 values are almost equal, as expected for the present experimental conditions, while SLPA predictions are much lower than the other two. Whatsoever, with a great surprise, we see that measured σ_K^I are at least a factor 2 higher than all the predictions. Note that the overall experimental uncertainty in the present cross-section measurements is attributed to the uncertainties in the photopeak, absolute efficiency of the detector, charge collected in Faraday cup, and target thickness.

The underestimation of the experimental data by the theoretical predictions provides a clear indication that the direct ionization process is not enough to explain the K-shell ionization phenomenon in the present experimental conditions and another important mechanism must be in action. Such a possibility can arise from electron capture phenomenon. K-K capture can be feasible if the K-shell of the projectile is either fully or partially vacant. Similarly, K-L capture will take place when L-shell of the projectile ion is unoccupied.

To calculate the K-K electron capture cross-sections,

we have used the theory of Lapicki and Losonsky [59] which is based on the Oppenheimer-Brinkman-Kramers (OBK) approximation [71] with binding and Coulomb deflection corrections at low velocities. Neglecting changes in the K-shell binding energy of the projectile with one versus two vacancies, a statistical scaling is used to relate the electron transfer cross-section of one ($\sigma_{1K \rightarrow K}$) and two ($\sigma_{2K \rightarrow K}$) K-shell vacancies as $\sigma_{1K \rightarrow K} \sim \sigma_{2K \rightarrow K}/2$. In the present experimental condition, $v_1 = 10.96 - 14.15$ and $v_{2K} = 28.7 - 31.7$ atomic units. Thus, the expression for $\sigma_{2K \rightarrow K}$ can be chosen as follows [59]:

$$\sigma_{2K \rightarrow K} = \frac{1}{3} \sigma_{2K \rightarrow K}^{OBK}(\theta_K), \quad (8)$$

where

$$\sigma_{2K \rightarrow K}^{OBK}(\theta_K) = \frac{2^9 \pi a_0^2}{5 v_1^2} \frac{(v_{1K} v_{2K})^5}{[v_{1K}^2 + (v_1^2 + v_{2K}^2 - v_{1K}^2)^2 / 4 v_1^2]^5}, \quad (9)$$

$$\theta_K = \frac{E_K}{Z_{2K}^2 \times 13.6}, \quad (10)$$

and $Z_{2K} = Z_2 - 0.3$. In Eq.(9), a_0 , v_{1K} , and v_{2K} are Bohr radius, K-shell orbital velocity for the projectile ion and target atom, respectively ; and E_K is the binding energy of the K-shell electron of the target in eV. Note that this K-K capture theory has been adapted to estimate the K-L capture cross-sections too.

In this work we deal with Si^{+14} and Si^{+13} , so the $\sigma_{1K \rightarrow K}$ and $\sigma_{2K \rightarrow K}$ are weighted with the charge state fractions $F(q)$, for $q=13$ and $q=14$. To obtain the $F(q)$ we have used the following methods: (i) *ab initio* approach by means of ETACHA4 code [58] and (ii) Fermi gas model based empirical formula [56]. It is worth noting that about a decade ago, the significance of the projectile charge state *inside* the target on the target ionization was not known at all. Thus, Horvat [25] has made use of the projectile charge state *outside* the target, which is incorrect as it will be evident after a while.

The ETACHA4 code, recently developed by Lamour et al [53], computes the charge state fractions of the projectile ions on the passage of a target medium, either solid or gas, by employing suitable rate equations. In the code, the non-radiative and radiative electron capture cross-sections are calculated using the relativistic eikonal approximation [72] and Bethe-Salpeter formula [73], respectively. The total electron capture cross-section is sum of the non-radiative and radiative electron capture cross-sections. Whereas, the ionization and excitation cross-sections are estimated using the continuum distorted-wave-eikonal initial state approximation [74, 75] and symmetric eikonal model [76, 77], respectively.

An important fact is that the excited states forming inside the solid target are mostly destroyed in the following collisions, in particular, if geometrical size of the excited states so created is larger than the lattice parameter of the target material. Whereas significant contribution of electron capture at the exit layers remains intact. This

is the reason, the excited state formation is considered to be occurring at the exit surface [78]. Hence, putting the electron capture cross-section equals to zero in the ETACHA4 code, provides us a good estimate of the CSD inside the solid target (CSD-I). This is important as CSD-I will be used later on to calculate the electron capture contribution in the K-shell ionization in the target atoms.

Instead, Horvat [25] in his ERCS08 code used an empirical formulae for the mean charge state, q_m , as well as CSD outside the target, CSD-O, by Schiwietz and Grande [57]. We emphasize here that this empirical values outside the target do not represent the quantities inside the target at all.

According to the Fermi gas model based empirical formula, the mean charge state (q_m) inside the target [56] is given by,

$$q_m = Z_1 \left(1 - \frac{v_F}{v_1}\right) \quad (11)$$

with Z_1 and v_F being the projectile atomic number and Fermi velocity of target electrons, respectively. Series of q_m -values obtained from x-ray spectroscopy experiments have been compared extremely well with the the above-mentioned formula [79]. Uncertainty of q_m is found to be $\approx 3\%$. The Fermi velocity v_F of Cu, Zn, and Ge are 1.11×10^6 , 1.566×10^6 [80] and 2.5×10^6 m/s [81], respectively.

To showcase the difference of ionization of the projectile ion inside and outside the target, we compare the q_m obtained from the Fermi gas model [56] with the empirical model by Schiwietz and Grande [57] (Schiwietz-Grande model). The Schiwietz-Grande model was developed from a large set of experimental charge-state distributions measured outside the solid target. We displayed the q_m as predicted by the Fermi gas model [56], and Schiwietz-Grande model [57] in Fig. 3. This contrasting picture is mostly governed by the solid surface [20, 21]. We also included in Fig. 3 the results of ETACHA4 code inside and outside the target. Clearly, the values of q_m outside the target are lower than inside in all the energy range studied here.

In second step, the q_m -values inside the target are substituted in the Lorentzian charge state distribution [19] to obtain the $F(q)$ as follows

$$F(q) = \frac{1}{\pi} \frac{\frac{\Gamma}{2}}{(q - q_m)^2 + (\frac{\Gamma}{2})^2} \text{ and } \sum_q F(q) = 1. \quad (12)$$

Here distribution width Γ is taken from Novikov and Teplova [82], as follows,

$$\Gamma(x) = C[1 - \exp(-(x)^\alpha)][1 - \exp(-(1-x)^\beta)]. \quad (13)$$

Here $x = q_m/Z_1$, $\alpha = 0.23$, $\beta = 0.32$, and $C = 2.669 - 0.0098Z_2 + 0.058Z_1 + 0.00048Z_1Z_2$. The $F(q)$ values so obtained are shown in Fig. 4(A) and the $F(q)$ for $q=13$ and 14 are displayed in a bar chart Fig. 4(B). Further, charge state fraction ($F(q)$) of Si^{13+}

and Si^{14+} obtained from FGM [56], ETACHA4 [58], and ERCS08 [25] in different target elements and at various kinetic energies of Si-ion beam are given in Table II. Note that FGM and ETACHA4 represent $F(q)$ inside the target, while ERCS08 gives the same outside the target, hence $F(q)$ from ERCS08 is not at all useful in understanding the vacancy production in target atoms by ion impact.

The σ_{KK} and σ_{KL} so obtained were added with the σ_K^I as obtained from direct ionization theories and plotted in Fig. 5. The improvement of the theoretical-experimental comparison from Fig. 2 (without capture) to Fig. 5 (ionization plus K-K and K-L capture) is very clear. These data are also given in Table III. The sum of direct ionization and K-K + K-L capture cross-sections show a good agreement with the corresponding experimental cross-sections. As can be noted in Fig. 5, ETACHA and FGM for this addition almost agree for Zn and Ge target, with differences for Cu. Furthermore, ECUSAR - FGM gives the closest agreement with the experimental data. Such overall agreement reveals that a simple Fermi gas model gives a correct estimation of the q_m inside the target, where v_F plays a central role and needs accurate evaluation.

Due to certain CSD inside the target, the charge state fraction for a specific q called $F(q)$ is an important quantity. The effective 2K-K OBK capture contribution in the present case is then equal to $F(q = 14) \times \sigma_{2k \rightarrow k}^{OBK}(\theta_k)$, for silicon ions. Similarly, to obtain effective K-K contribution $F(q = 13)$ will be required. Note that ERCS08 [25] code takes the charge state fractions of the projectile ions outside the target [57]

We tested the above mentioned approach by re-analysing earlier data for C- and Si-ion on Ti target at much lower energies. Details and the excellent results obtained are included in Appendix V, and reinforce the present conclusions.

To deepen our study about which theoretical method gives the best representation of the experimental data, we have compared the total electron capture cross-section obtained from different theoretical approaches in Fig. 6. Here, we see that the electron capture cross-sections almost follow the mean charge state behavior shown in Fig. 4. Further, the electron capture cross-sections are close if the charge state fractions are taken from FGM [56] and ETACHA4 [58]. Therefore, either FGM or ETACHA4 can be used to estimate the projectile charge state distribution inside the solid target. However, ETACHA4 can handle up to a certain number of electrons in the projectile ion and thus difficulties arise in applying this for heavy projectiles. Whereas no such restrictions with the FGM. Electron capture cross-sections obtained from the ERCS08 is very low as the charge state distribution outside the target is considered there.

IV. CONCLUSION

We have demonstrated the contribution of electron capture in K-shell ionization by heavy-ion impact. Here, the targets Cu, Zn, and Ge were bombarded by the 84-140 MeV ^{28}Si ions to measure K-shell production cross-sections. We observed that the measured ionization cross-sections differ at least a factor of two from the theoretical direct ionization cross-sections. Electron capture from the target K-shell to the K- and L-shell of the projectile ions was required to resolve this difference. In this regard, projectile charge state inside the target is extremely essential. Use of mean charge state from a Fermi gas model [56] and distribution width from Novikov and Teplova formula [82] in the Lorentzian charge state distribution [18] lead to obtaining the charge state distributions. The bare and H-like projectile ions inside the targets have been utilised to calculate the K-K capture contribution from Lapicki and Losonsky [59]. While all the charge state fractions are used for K-L capture calculations. Sum of the theoretically calculated direct ionization cross-section and K-K + K-L capture cross-sections represent pretty well the experimentally measured values.

In order to validate the above mentioned approach, we have reanalysed the earlier data for C- and Si-ion on Ti target at much lower energies. Hence, in this study we have not only succeeded in studying the dynamics of K-shell ionization, but also succeeded in correctly estimating the charge state distribution inside the targets using a simple Fermi gas model. Further, we have shown that the mean charge state inside the foil is much higher than that outside it. Thus, the exit surface plays a significant role in changing charge state from a higher to lower one. Such a knowledge can be put into application to obtain a high charge state from a foil stripper if the electron capture phenomena at the stripper surface is restricted. Quasi-free electrons at the conducting surface can be captured easily with the exiting ions. Whereas such scope is remote from the insulating surface. Hence, a special surface engineering can be applied to make a target surface from conducting to insulating one for obtaining the higher charge states.

V. ACKNOWLEDGEMENTS

We acknowledge cooperation from the Pelletron accelerator staff during the experiments. SC acknowledges the University of Kalyani for providing generous funding towards his fellowship. CCM acknowledges the financial support by CONICET and PICT2017-2945 from Argentina.

Appendix

Validation of the theoretical method

The theoretical approach so developed has been validated through earlier experimental results of Si ion on Ti [32] and shown in Fig. 7 and Table IV. It is observed there [32] that C-data agree well with ECPSSR predictions [83] but Si-data are 30 to 15 times higher than the ECPSSR estimations in the energy range of 10-20 MeV. Inclusion of SMI with ECUSAR calculation for accounting direct ionisation exhibits nearly the same scenario, but molecular orbital (MO) theory [60] improves the results to a some extent at this low energies < 1 MeV/u, but still away from the observed scenario. Next, to take K-K and K-L capture cross-sections [59] into consideration, we find the q_m inside the target by the Fermi gas model [56]. Values so obtained are compared with that outside the target using the Schiweitz model [57] is shown in Fig. 7 A. Note that Fermi velocity of Ti is taken as 1.38×10^6 m/s [81]. The CSD inside the target is depicted at different energies in Fig. 7 B. Corresponding charge state fractions for $q = 13+$ and $14+$ as shown in Fig. 7 C are used in the K-K capture cross-section [59]. Finally, different theoretical values are compared in Fig. 7 D, where the sum of the K-K + K-L capture cross-section [59] and the ECUSAR cross-section agrees within 25%

with the experimental data except a larger difference ($\approx 45\%$) at the lowest energy where the photopeak is very weak and thus background might have been underrated. Further, measurement uncertainty is not quoted there. Whatsoever, this excellent agreement is achieved because of 30-15 times higher contribution from electron capture than that from direct ionization in Ti atoms comes as we move from 10 to 20 MeV energy of Si-projectiles.

TABLE IV: Theoretical direct ionization cross-section obtained from ECUSAR including simultaneous multiple ionization (σ_{DI}), molecular orbital (MO) cross-section (σ_{MO}) [60], K-K capture cross-section [59] for $13+$ (σ_{K-K}^{13+}) and $14+$ charge state (σ_{K-K}^{14+}) from FGM, total capture cross-section plus MO cross-section ($\sigma_{Tot} = \sigma_{DI} + \sigma_{K-K}$) and experimental ionization cross-section (σ_K^I) for Ti target by the ^{28}Si ions of different energies (E_1 MeV) [32] are listed in units of barns/atom. Note that measurement uncertainty is not mentioned there.

Ti (Experimental data from [32])						
E_1 MeV	σ_{DI}	σ_{MO}	EC		σ_{Tot}	σ_K^I (Exptl.)
			K-K	K-L		
10	2	8	16	17	35	66
15	20	57	235	117	372	286
20	108	209	1412	354	1874	1481

-
- [1] J. Miranda, O. De Lucio, and M. Lugo-Licona, *Revista mexicana de física* **53**, 29 (2007).
- [2] G. Kraft, *Progress in particle and Nuclear Physics* **45**, S473 (2000).
- [3] E. Sternglass, *Physical Review* **108**, 1 (1957).
- [4] Z. Vager and D. S. Gemmell, *Physical Review Letters* **37**, 1352 (1976).
- [5] A. Lifschitz and N. Arista, *Physical Review A* **69**, 012902 (2004).
- [6] G. Lapicki and F. D. McDaniel, *Physical Review A* **22**, 1896 (1980).
- [7] E. C. Stone, A. Frandsen, R. Mewaldt, E. Christian, D. Margolies, J. Ormes, and F. Snow, *Space Science Reviews* **86**, 1 (1998).
- [8] G. Gloeckler, J. Cain, F. Ipavich, E. Tums, P. Bedini, L. Fisk, T. Zurbuchen, P. Bochsler, J. Fischer, R. Wimmer-Schweingruber, *et al.*, in *The advanced composition explorer mission* (Springer, 1998) pp. 497-539.
- [9] S. Lepri and T. Zurbuchen, *The Astrophysical Journal Letters* **723**, L22 (2010).
- [10] J. Lindl, *Physics of plasmas* **2**, 3933 (1995).
- [11] L. Young, E. P. Kanter, B. Krässig, Y. Li, A. March, S. Pratt, R. Santra, S. Southworth, N. Rohringer, L. DiMauro, *et al.*, *Nature* **466**, 56 (2010).
- [12] S. Vinko, O. Ciricosta, B. Cho, K. Engelhorn, H.-K. Chung, C. Brown, T. Burian, J. Chalupský, R. Falcone, C. Graves, *et al.*, *Nature* **482**, 59 (2012).
- [13] B. Rudek, S.-K. Son, L. Foucar, S. W. Epp, B. Erk, R. Hartmann, M. Adolph, R. Andritschke, A. Aquila, N. Berrah, *et al.*, *Nature photonics* **6**, 858 (2012).
- [14] P. Stier, C. Barnett, and G. Evans, *Physical Review* **96**, 973 (1954).
- [15] C. Moak, *Phys. Rev* **176**, 427 (1968).
- [16] H. D. Betz and L. Grodzins, *Physical Review Letters* **25**, 211 (1970).
- [17] J. A. Nolen and F. Marti, *Reviews of Accelerator Science and Technology* **6**, 221 (2013).
- [18] P. Sharma and T. Nandi, *Physics Letters A* **380**, 182 (2016).
- [19] P. Sharma and T. Nandi, *Physics of Plasmas* **23**, 083102 (2016).
- [20] P. Sharma and T. Nandi, *Physical Review Accelerators and Beams* **22**, 034501 (2019).
- [21] T. Nandi, *The Astrophysical Journal Letters* **673**, L103 (2008).
- [22] C. C. Montanari and P. Dimitriou, *Nuclear Instruments and Methods in Physics Research Section B: Beam Interactions with Materials and Atoms* **408**, 50 (2017).
- [23] G. Lapicki, G. R. Murty, G. N. Raju, B. S. Reddy, S. B. Reddy, and V. Vijayan, *Physical Review A* **70**, 062718 (2004).
- [24] C. Montanari and J. Miraglia, *Advances in Quantum Chemistry* **65**, 165 (2013).
- [25] V. Horvat, *Computer Physics Communications* **180**, 995 (2009).

- [26] M. O. Krause, *Journal of physical and chemical reference data* **8**, 307 (1979).
- [27] O. Benka and A. Kropf, *Atomic Data and Nuclear Data Tables* **22**, 219 (1978).
- [28] I. Orlic, C. Sow, and S. Tang, *Atomic data and nuclear data tables* **56**, 159 (1994).
- [29] U. Kadhane, C. Montanari, and L. C. Tribedi, *Physical Review A* **67**, 032703 (2003).
- [30] G. Lapicki, *X-Ray Spectrometry: An International Journal* **34**, 269 (2005).
- [31] X. Zhou, Y. Zhao, R. Cheng, Y. Wang, Y. Lei, X. Wang, and Y. Sun, *Nuclear Instruments and Methods in Physics Research Section B: Beam Interactions with Materials and Atoms* **299**, 61 (2013).
- [32] M. Msimanga, C. Pineda-Vargas, and M. Madhuku, *Nuclear Instruments and Methods in Physics Research Section B: Beam Interactions with Materials and Atoms* **380**, 90 (2016).
- [33] S. Kumar, U. Singh, M. Oswal, G. Singh, N. Singh, D. Mehta, T. Nandi, and G. Lapicki, *Nuclear Instruments and Methods in Physics Research Section B: Beam Interactions with Materials and Atoms* **395**, 39 (2017).
- [34] M. Oswal, S. Kumar, U. Singh, G. Singh, K. Singh, D. Mehta, D. Mitnik, C. C. Montanari, and T. Nandi, *Nuclear Instruments and Methods in Physics Research Section B: Beam Interactions with Materials and Atoms* **416**, 110 (2018).
- [35] M. Hazim, C. Koumeir, A. Guertin, V. Métivier, A. Naja, N. Servagent, and F. Haddad, *Nuclear Instruments and Methods in Physics Research Section B: Beam Interactions with Materials and Atoms* **479**, 120 (2020).
- [36] M. Oswal, S. Kumar, U. Singh, S. Singh, G. Singh, K. Singh, D. Mehta, A. Mendez, D. Mitnik, C. Montanari, et al., *Radiation Physics and Chemistry* **176**, 108809 (2020).
- [37] J. Miranda, D. Serrano, J. Pineda, D. Marín-Lámbarri, L. Acosta, J. Mendoza-Flores, S. Reynoso-Cruces, and E. Chávez, *Nuclear Instruments and Methods in Physics Research Section B: Beam Interactions with Materials and Atoms* **477**, 23 (2020).
- [38] P. Dahl, M. Rodbro, G. Hermann, B. Fastrup, and M. Rudd, *Journal of Physics B: Atomic and Molecular Physics* **9**, 1581 (1976).
- [39] M. Pajek, D. Banaś, J. Semaniak, J. Braziewicz, U. Majewska, S. Chojnacki, T. Czyżewski, I. Fijał, M. Jaskóła, A. Glombik, et al., *Physical Review A* **68**, 022705 (2003).
- [40] L. Sarkadi and T. Mukoyama, *Journal of Physics B: Atomic and Molecular Physics* **14**, L255 (1981).
- [41] V. Maidikov, N. Surovitskaya, N. Skobelev, and W. Neubert, *Nuclear Instruments and Methods in Physics Research* **192**, 205 (1982).
- [42] M. Leino, J. Äystö, T. Enqvist, P. Heikkinen, A. Jokinen, M. Nurmi, A. Ostrowski, W. Trzaska, J. Uusitalo, K. Eskola, P. Armbruster, and V. Ninov, *Nuclear Instruments and Methods in Physics Research Section B: Beam Interactions with Materials and Atoms* **99**, 659 (1995), application of Accelerators in Research and Industry '94.
- [43] J. Khuyagbaatar, D. Ackermann, L.-L. Andersson, J. Ballof, W. Bröchle, C. Düllmann, J. Dvorak, K. Eberhardt, J. Even, A. Gorshkov, R. Graeger, F.-P. Heßberger, D. Hild, R. Hoischen, E. Jäger, B. Kindler, J. Kratz, S. Lahiri, B. Lommel, M. Maiti, E. Merchan, D. Rudolph, M. Schädel, H. Schaffner, B. Schausten, E. Schimpf, A. Semchenkov, A. Serov, A. Türler, and A. Yakushev, *Nuclear Instruments and Methods in Physics Research Section A: Accelerators, Spectrometers, Detectors and Associated Equipment* **1010**, 165301 (2016).
- [44] T. Dickel, W. Plaß, S. Ayet San Andres, J. Ebert, H. Geissel, E. Haettner, C. Hornung, I. Miskun, S. Pietri, S. Purushothaman, M. Reiter, A.-K. Rink, C. Scheidenberger, H. Weick, P. Dendooven, M. Diwisch, F. Greiner, F. Heiße, R. Knöbel, W. Lippert, I. Moore, I. Pohjalainen, A. Prochazka, M. Ranjan, M. Takechi, J. Winfield, and X. Xu, *Physics Letters B* **744**, 137 (2015).
- [45] H. Sa'adeh, R. Ali, and D.-E. Arafah, *Nuclear Instruments and Methods in Physics Research Section B: Beam Interactions with Materials and Atoms* **269**, 2111 (2011).
- [46] S. K. Allison, *Rev. Mod. Phys.* **30**, 1137 (1958).
- [47] A. Wittkower and H. Betz, *Atomic Data and Nuclear Data Tables* **5**, 113 (1973).
- [48] K. Shima, T. Mikumo, and H. Tawara, *Atomic Data and Nuclear Data Tables* **34**, 357 (1986).
- [49] K. Shima, N. Kuno, M. Yamanouchi, and H. Tawara, *Atomic Data and Nuclear Data Tables* **51**, 173 (1992).
- [50] N. Bohr, *Physical Review* **59**, 270 (1941).
- [51] V. Nikolaev and I. Dmitriev, *Physics Letters A* **28**, 277 (1968).
- [52] K. To and R. Drouin, *Physica Scripta* **14**, 277 (1976).
- [53] K. Shima, T. Ishihara, and T. Mikumo, *Nuclear Instruments and Methods in Physics Research* **200**, 605 (1982).
- [54] A. Itoh, H. Tsuchida, T. Majima, A. Yogo, and A. Ogawa, *Nuclear Instruments and Methods in Physics Research Section B: Beam Interactions with Materials and Atoms* **159**, 22 (1999).
- [55] G. Schiwietz, K. Czerski, M. Roth, F. Staufenbiel, and P. Grande, *Nuclear Instruments and Methods in Physics Research Section B: Beam Interactions with Materials and Atoms* **225**, 4 (2004).
- [56] W. Brandt, R. Laubert, M. Mourino, and A. Schwarzschild, *Physical Review Letters* **30**, 358 (1973).
- [57] G. Schiwietz and P. Grande, *Nuclear Instruments and Methods in Physics Research Section B: Beam Interactions with Materials and Atoms* **175**, 125 (2001).
- [58] E. Lamour, P. D. Fainstein, M. Galassi, C. Prigent, C. A. Ramirez, R. D. Rivarola, J.-P. Rozet, M. Trassinelli, and D. Vernhet, *Phys. Rev. A* **92**, 042703 (2015).
- [59] G. Lapicki and W. Losonsky, *Physical Review A* **15**, 896 (1977).
- [60] E. Montenegro and G. Sigaud, *Journal of Physics B: Atomic and Molecular Physics* **18**, 299 (1985).
- [61] E. Subramaniam and B. Kumar, *Nucl. Phys* **117** (2010).
- [62] D. Burch, L. Wilets, and W. Meyerhof, *Physical Review A* **9**, 1007 (1974).
- [63] E. Choi, E. Merzbacher, and G. Khandelwal, *Atomic Data and Nuclear Data Tables* **5**, 291 (1973).
- [64] W. Brandt and G. Lapicki, *Physical Review A* **23**, 1717 (1981).
- [65] C. B.ucci, R. F.iesh, and J. H.lroh, *Physical Review* **90**, 659 (1953), Beam Interactions with Materials and Atoms (1995), Effects and Defects in Solids **166**, 338 (2011).
- [66] Z. H. Levine and S. G. Louie, *Physical Review B* **25**, 6310 (1982).
- [67] E. Clementi and C. Roetti, *Atomic data and nuclear data tables* **14**, 177 (1974).
- [68] U. Kadhane, C. Montanari, and L. C. Tribedi, *Journal of Physics B: Atomic, Molecular and Optical Physics* **36**, 3043 (2003).

- [69] C. Montanari, P. Miranda, E. Alves, A. Mendez, D. Mitnik, J. Miraglia, R. Correa, J. Wachter, M. Aguilera, N. Catarino, *et al.*, *Physical Review A* **101**, 062701 (2020).
- [70] C. C. Montanari and J. E. Miraglia, *Physical Review A* **96**, 012707 (2017).
- [71] R. May, *Physics Letters* **11**, 33 (1964).
- [72] W. E. Meyerhof, R. Anholt, J. Eichler, H. Gould, C. Munger, J. Alonso, P. Thieberger, and H. E. Wegner, *Phys. Rev. A* **32**, 3291 (1985).
- [73] H. A. Bethe and E. E. Salpeter, *Encyclopedia of Physics* **35** (1957).
- [74] P. D. Fainstein, V. H. Ponce, and R. D. Rivarola, *Physical Review A* **36**, 3639 (1987).
- [75] P. Fainstein, V. H. Ponce, and R. D. Rivarola, *Journal of Physics B: Atomic, Molecular and Optical Physics* **24**, 3091 (1991).
- [76] G. H. Olivera, C. A. Ramírez, and R. D. Rivarola, *Physical Review A* **47**, 1000 (1993).
- [77] C. A. Ramírez and R. D. Rivarola, *Physical Review A* **52**, 4972 (1995).
- [78] N. Tolk, L. C. Feldman, J. Kraus, J. Tully, M. Hass, Y. Niv, and G. Temmer, *Physical Review Letters* **47**, 487 (1981).
- [79] T. Nandi, P. Sharma, and P. Kumar, arXiv preprint arXiv:1905.04328 (2019).
- [80] D. Gall, *Journal of Applied Physics* **119**, 085101 (2016).
- [81] D. Isaacson, New York University, Document (1975).
- [82] N. Novikov and Y. A. Teplova, *Physics Letters A* **378**, 1286 (2014).
- [83] W. Brandt and G. Lapicki, *Physical Review A* **20**, 465 (1979).

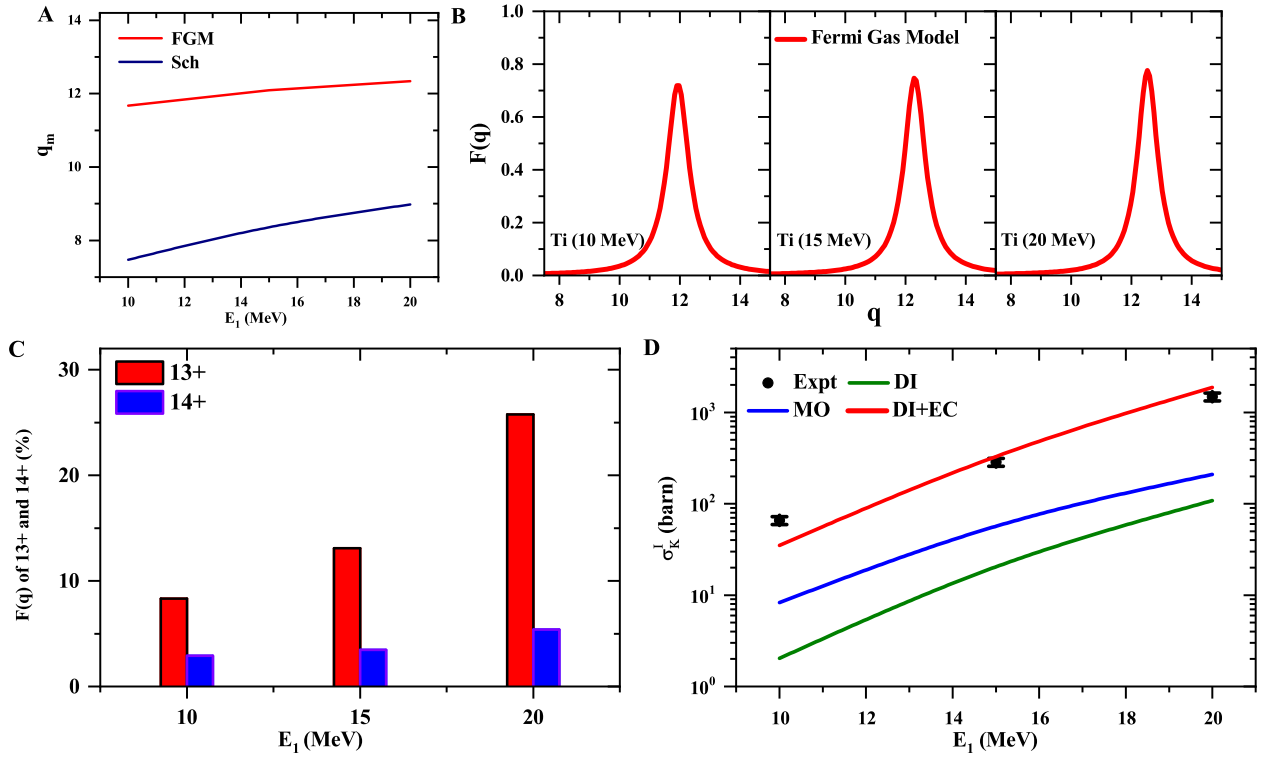


FIG. 7: (A)-(C) are same as Fig. 3 and 4 but for *Ti* target and data taken from [32]. (D) comparison of experimental K shell ionization cross-sections with the ECUSAR (DI) [23], molecular orbital (MO) cross-sections [60] and the sum of the DI and electron capture (EC) cross-sections [59] versus ion-beam energies.